Clinical Neurophysiology 132 (2021) 382–391

Contents lists available at ScienceDirect

Clinical Neurophysiology

journal homepage: www.elsevier.com/locate/clinph

Noninvasive measurement of sensory action currents in the cervical cord by magnetospinography

Miho Akaza [a], Shigenori Kawabata [b,*], Isamu Ozaki [c], Yuki Miyano [d], Taishi Watanabe [d], Yoshiaki Adachi [e], Kensuke Sekihara [b], Yuki Sumi [a], Takanori Yokota [f]

[a] Respiratory and Nervous System Science, Biomedical Laboratory Science, Graduate School of Medical and Dental Sciences, Tokyo Medical and Dental University, 1-5-45 Yushima, Bunkyo-ku, Tokyo 113-8519, Japan
[b] Department of Advanced Technology in Medicine, Graduate School of Medical and Dental Sciences, Tokyo Medical and Dental University, 1-5-45 Yushima, Bunkyo-ku, Tokyo 113-8519, Japan
[c] Department of Physical Therapy, Faculty of Health Sciences, Aomori University of Health and Welfare, 58-1 Mase, Hamadate, Aomori 030-8505, Japan
[d] Healthcare Business Group, RICOH Company, Ltd., 2-3-10 Kandasurugadai Chiyoda-ku, Tokyo 101-0062, Japan
[e] Applied Electronics Laboratory, Kanazawa Institute of Technology, 7-1 Ogigaoka, Nonoichi, Ishikawa 921-8501, Japan
[f] Department of Neurology and Neurological Science, Graduate School of Medical and Dental Sciences, Tokyo Medical and Dental University, 1-5-45 Yushima, Bunkyo-ku, Tokyo 113-8519, Japan

ARTICLE INFO

Article history:
Accepted 6 November 2020
Available online 19 December 2020

Keywords:
Magnetospinography
Superconducting quantum interference device (SQUID)
Evoked magnetic field
Dorsal column
Dorsal horn
Somatosensory evoked potential

HIGHLIGHTS

- Neural activity in the cervical cord and root evoked by median nerve wrist stimulation can be visualized by magnetospinography.
- Dorsal horn excitatory postsynaptic activity can also be identified by magnetospinography.
- Magnetospinography provides useful information for the functional electrophysiological diagnosis of somatosensory pathways.

ABSTRACT

Objective: To obtain magnetic recordings of electrical activities in the cervical cord and visualize sensory action currents of the dorsal column, intervertebral foramen, and dorsal horn.
Methods: Neuromagnetic fields were measured at the neck surface upon median nerve stimulation at the wrist using a magnetospinography system with high-sensitivity superconducting quantum interference device sensors. Somatosensory evoked potentials (SEPs) were also recorded. Evoked electrical currents were reconstructed by recursive null-steering beamformer and superimposed on cervical X-ray images.
Results: Estimated electrical currents perpendicular to the cervical cord ascended sequentially. Their peak latency at C5 and N11 peak latency of SEP were well-correlated in all 16 participants ($r = 0.94$, $p < 0.0001$). Trailing axonal currents in the intervertebral foramens were estimated in 10 participants. Estimated dorsal–ventral electrical currents were obtained within the spinal canal at C5. Current density peak latency significantly correlated with cervical N13–P13 peak latency of SEPs in 13 participants ($r = 0.97$, $p < 0.0001$).
Conclusions: Magnetospinography shows excellent spatial and temporal resolution after median nerve stimulation and can identify the spinal root entry level, calculate the dorsal column conduction velocity, and analyze segmental dorsal horn activity.
Significance: This approach is useful for functional electrophysiological diagnosis of somatosensory pathways.

Abbreviations: SCEF, spinal cord evoked magnetic fields; SEP, somatosensory evoked potential; MSG, magnetospinography; SQUID, superconducting quantum interference device; DSSP, dual signal subspace projection; UGRENS, unit gain constraint recursively applied null-steering spatial filtering.

* Corresponding author at: Department of Advanced Technology in Medicine, Graduate School of Tokyo Medical and Dental University, 1-5-45 Yushima, Bunkyo-ku, Tokyo 113-8510, Japan.

E-mail addresses: m-akaza.nuro@tmd.ac.jp (M. Akaza), kawabata.orth@tmd.ac.jp (S. Kawabata), isamu_ozaki@icloud.com (I. Ozaki), yuki.yh.hasegawa@jp.ricoh.com (Y. Miyano), taishi.watanabe@jp.ricoh.com (T. Watanabe), k-sekihara@nifty.com (K. Sekihara), ysumi.pulm@tmd.ac.jp (Y. Sumi), tak-yokota.nuro@tmd.ac.jp (T. Yok.

https://doi.org/10.1016/j.clinph.2020.11.029
1388-2457/

1. Introduction

Paresthesia and sensory deficit of the hands are some of the most common symptoms of both cervical spinal cord diseases and peripheral neuropathies. Although conventional noninvasive electrophysiological techniques such as somatosensory evoked potentials (SEPs) are useful for detecting functional abnormalities of the somatosensory pathways, they are incapable of assessing the exact site of conduction failure in the dorsal column. The ascending dorsal column activity after median nerve stimulation at the wrist can be detected as a small positive potential (P11) that is recorded from the scalp with reference to the hand, shoulder, or clavicle contralateral to the stimulation (a non-cephalic montage) and that culminates at around 11 ms after the stimulus (Cracco and Cracco, 1976; Cruccu et al., 2008; Desmedt and Cheron, 1980). This activity corresponds to a small negative potential (N11) that is recorded at the skin surface of the posterior neck with a non-cephalic montage (Desmedt and Cheron, 1980; Desmedt and Nguyen, 1984). However, this near-field N11 potential is often ill-defined because it appears during the transition from a positive potential of the brachial plexus origin (P9) to a negative potential of the dorsal horn origin (cervical N13). Furthermore, the P11 potential is reported to be indiscernible in about one-third of healthy individuals (Ozaki et al., 1994; Tanosaki et al., 1999), probably because the electrophysiological heterogeneity of the surrounding vertebral bones and soft tissues may distort the extracellular current distribution of the action potential.

In contrast to potential recording, magnetic recordings are not influenced by the bone and skin (Hashimoto et al., 1991; Trahms et al., 1989). This results in magnetic distributions with a smaller spatial extent. Since 1999, our group has been working on magnetospinography (MSG) to noninvasively assess spinal cord and deep nerve dysfunction. There have since been several reports on animal experiments concerning neuromagnetic fields of the cervical spinal cord after stimulation of the lower thoracic cord, called cervical spinal cord evoked magnetic fields (cervical SCEFs), which demonstrate propagation of ascending volleys along the spinal cord and conduction block at the experimental cord lesion in cats (Kawabata et al., 2002) and rabbits (Tomori et al., 2010). Ascending volleys and synaptic activity in the lumbar spinal cord have also been distinguished by analyzing SCEFs after stimulation of the sciatic nerve in rabbits (Tomizawa et al., 2008). In addition, Sumiya et al. (2017) successfully recorded cervical SCEFs at the body surface in humans after stimulation of the lower thoracic cord with an epidural electrode to estimate the current constitution of the nerve impulse that travels along the cervical cord. Moreover, the results of cervical SCEFs in a patient with cervical spondylotic myelopathy that were overlaid on the patient's cervical X-ray image showed that the site of the impulse travel failure coincided with the site of cervical spinal stenosis, demonstrating that MSG can be clinically applied to spinal cord functional tests (Sumiya et al., 2017).

However, to expand the clinical application of cervical SCEFs, a noninvasive procedure would be preferred, particularly one that avoids the need for epidural electrode insertion. For examination of upper limb stimulation, electrical stimulation at the elbow might be more useful than stimulation at the wrist for recording sufficiently large signals of cervical SCEFs. Thus, in their study, Sumiya et al. (2017) attempted to record cervical SCEFs after electrical stimulation of the median nerve at the elbow in healthy individuals and were able to delineate the ascending volley along the dorsal column and action potentials at the dorsal root entry zone as chronological current constitution maps that were estimated from the cervical SCEFs. However, it remains to be determined whether median nerve stimulation at the wrist in healthy individuals can evoke cervical SCEFs with a high signal-to-noise ratio that permits evaluation of the dorsal column volley, dorsal horn excitatory postsynaptic activity, and action potentials at the dorsal root entry zone.

Therefore, in the present study, we attempted to measure the magnetic field at the neck in response to electrical stimulation of the median nerve at the wrist and reconstructed the chronological current distribution in the cervical cord to visualize the ascending volley along the dorsal column, dorsal horn excitatory postsynaptic activity, and action potentials at the dorsal root entry zone. We also recorded conventional SEPs at the skin surface of the anterior and posterior neck regions with a non-cephalic montage to determine the relationship between the cervical N11 potential and the dorsal column activity reconstructed from magnetic fields or between dorsal horn activity, including the posterior neck N13 potential and anterior neck P13 potential, and its magnetic counterpart that may be localized within the spinal cord.

2. Methods

2.1. Standard protocol approvals, registration, and patient consent

This study was approved by the Ethics Committee of Tokyo Medical and Dental University of Medicine (#M2000-1229). All participants provided written informed consent.

2.2. MSG system

All recordings were performed using a multichannel superconducting quantum interference device (SQUID) biomagnetometer system developed by the Applied Electronics Laboratory, Kanazawa Institute of Technology (Adachi et al., 2017). The device is equipped with an array of 44 SQUID magnetometers arranged in an area of 180 mm × 130 mm (Fig. 1A) along the cylindrical surface with a 200-mm radius, as shown in Fig. 1B. Vector-type SQUID magnetometers, which simultaneously detect three orthogonal components of magnetic fields (Fig. 1D), were applied to extract as much magnetic field information from the observation area as possible. The sensors positioned at the four corners of the sensor array marked in gray-filled circles in Fig. 1a detected only the Z-component of the measurements from some of the participants due to the limit in the number of data acquisition channels. The noise level in the white noise region was typically less than 4 $fT/Hz^{0.5}$.

A cryostat was specifically designed to maintain the SQUID sensors in their superconducting state (Fig. 1C). It has a cylindrical main body to store liquid helium and a protrusion from its side surface. The sensor array was installed along the upper surface of the protrusion and oriented upward to detect the biomagnetic field along the back surface of participants in the supine position. In this article, the x-, y-, and z-directions were considered to be oriented from the left to right, from the caudal to cranial, and from the ventral to dorsal side of the body, respectively.

2.3. Signal processing

Although artifacts due to the electrical stimulation during the measurement often make it difficult to analyze the signal in the early latency period after stimulation, the artifact-removal method dual signal subspace projection (DSSP) (Sekihara et al., 2016) was able to effectively suppress artifacts. Unit gain constraint recursively applied null-steering spatial filtering (UGRENS) (Kumihashi and Sekihara, 2010; Sekihara and Nagarajan, 2015) was adapted to the acquired magnetic field data to reconstruct the spatial distribution of the current density around the spinal cord. The reconstructed current distribution obtained was superimposed on an

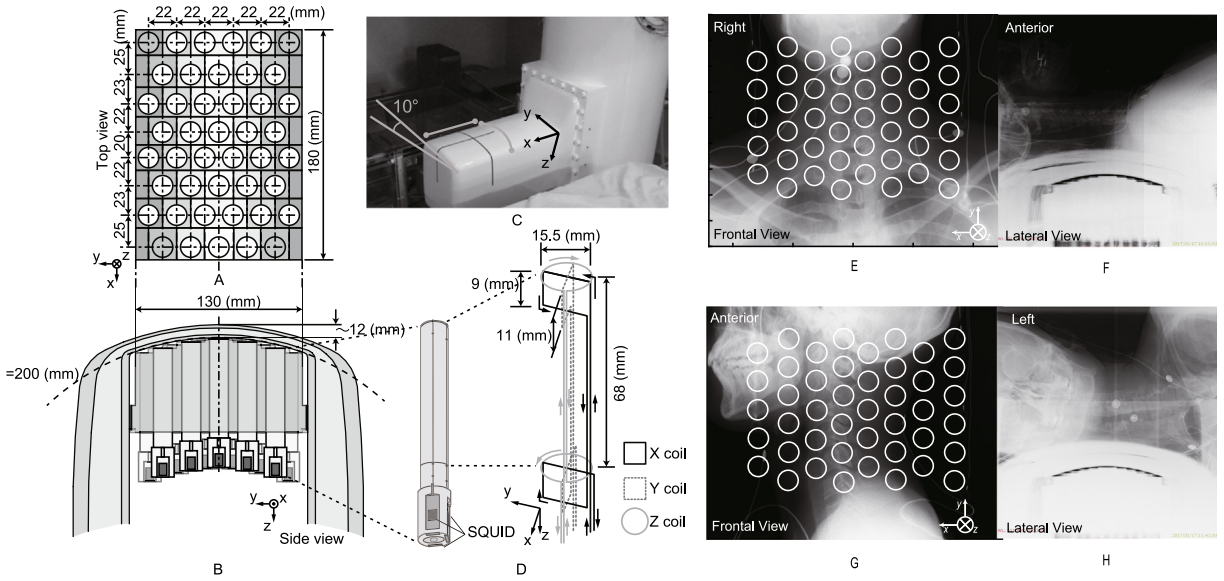

Fig. 1. Appearance and structure of the magnetospinography system. (A, B) The device is equipped with an array of 44 superconducting quantum interference device (SQUID) magnetometers arranged in an area of 180 mm × 130 mm along the cylindrical surface with a 200-mm radius. The sensors positioned at the four corners of the sensor array marked using gray-filled circles detected only the Z-component during the measurement of some of the participants due to the limit on the number of data acquisition channels. The noise level in the white noise region is typically less than 4 fT/Hz$^{0.5}$. (C, D) The cryostat to maintain the SQUID sensors in their superconducting state has uniquely designed vector-type SQUID magnetometers, which simultaneously detect three orthogonal components of the magnetic fields and are applied to extract the maximum possible amount of magnetic field information from the observation area. It has a cylindrical main body to store liquid helium and a protrusion from its side surface. The sensor array is installed along the upper surface of the protrusion oriented upward to observe the biomagnetic field along the back surface of participants in the supine position. (E, F) X-ray images in the frontal view (E) and lateral view (F) show the relationship between the sensors and the participant in Experiment 1. (G, H) X-ray images in the frontal view (G) and lateral view (H) show the relationship between the sensors and the participant in Experiment 2.

X-ray image for coregistration with morphological information. The position of the spinal cord relative to the sensor array was determined based on the lateral X-ray image. The depth of the source was estimated using the distance between the midpoint of the spinal canal and the center of the sensor array. The reconstructed current can be obtained from the magnetic field distribution at each measured time point. According to this method, it is possible to display a temporal change in the current intensity at any location, such as the spinal canal or the foramen, in a specific time domain as a waveform as if a virtual electrode was placed there.

2.4. Experiment 1. Recording of the magnetic field from the surface of the posterior neck in response to electrical supramaximal median nerve stimulation at the wrist

Sixteen healthy volunteers aged 25–42 years (mean ± SD, 33.5 ± 5.5 years) and measuring 156–182 cm in height (mean ± SD, 169.2 ± 7.0 cm) participated in Experiment 1. Recordings were performed with the participants in the supine position. The relationship between the sensors and the participant is shown in Fig. 1E and F. The distance between the sensors and the cervical cord was minimized. Neuromagnetic fields in response to electrical supramaximal stimulation (duration, 0.3 ms at 2–5 Hz) of the right-side median nerve at the wrist were measured at the surface of the posterior neck using the above-mentioned MSG system. Evoked responses synchronized with the stimulation were acquired at a sampling rate of 40 kHz with 100 Hz to 5 kHz analog band-pass filtering. The high-frequency band-pass filter was set to 100 Hz to eliminate artifacts and evaluate axonal electrical activity in the dorsal column. Our group previously reported that, with this setting, intra-axonal currents and inward volume currents at the depolarization site could be evaluated in the cervical cord and peripheral nerves in the cauda equina, brachial plexus, and median nerve around the carpal tunnel (Sumiya et al., 2017; Ushio et al., 2019; Watanabe et al., 2019; Sasaki et al., 2020). Two thousand responses from −5 to 30 ms after the stimulation were averaged to improve the signal-to-noise ratio and the evoked action currents were reconstructed by the above-mentioned spatial filter—a recursive null-steering (RENS) beamformer—and superimposed on an X-ray image of each participant's cervical spine.

2.5. Experiment 2. Recording of the magnetic field from the right side of the neck in response to electrical supramaximal median nerve stimulation at the wrist

Thirteen healthy volunteers aged 25–42 years (mean ± SD, 33.2 ± 5.5 years) and measuring 156–178 cm in height (mean ± SD, 168.4 ± 6.4 cm) participated in Experiment 2. Because the dorsal horn excitatory postsynaptic activity runs from dorsal to ventral, recordings were performed with the participants in the right lateral decubitus position. The relationship between the sensors and the participant is shown in Fig. 1G and H. The distance between the sensors and the cervical cord was minimized. Neuromagnetic fields were measured at the surface of the right-side neck in response to electrical supramaximal stimulation (duration, 0.3 ms at 2–5 Hz) of the right-side median nerve at the wrist. Evoked responses were acquired at a sampling rate of 40 kHz with 10 Hz to 5 kHz analog band-pass filtering. In contrast to Experiment 1, the high-frequency band-pass filter was set to 10 Hz to evaluate the dorsal horn excitatory postsynaptic activity. Two thousand responses from −5 to 30 ms after the stimulation were averaged, and evoked action currents were reconstructed by a spatial filter—a RENS beamformer—and superimposed on a lateral X-ray image of each participant's cervical spine, as in Experiment 1.

2.6. SEP recording

Immediately before each magnetic field measurement, a conventional SEP with the same stimulus setting was also recorded

in the supine position for reference. The SEP recording electrodes (impedance, <5 kΩ; filter bandpass, 20–2000 Hz) were set at the right–left Erb's point, C5 posterior (C5S)–left Erb's point, and C5 posterior–anterior cervical (AC) derivation. In three participants, a C3′ (2 cm posterior to C3)–Fz montage, C3′–left Erb's point montage, and Fz–left Erb's point montage were also recorded. More than 300 responses were averaged, and the SEP measurement was repeated at least twice to confirm reproducibility. An MEB2300 neuropack device (Nihon Kohden, Tokyo, Japan) was used to record SEPs and stimulate the nerve for the MSG and SEP measurement.

2.7. Analysis

When a nerve is electrically stimulated, transmembrane ionic currents are generated at the depolarization site in the nerve. Accordingly, intra-axonal and inward volume currents at the depolarization site are derived from the voltage difference between the depolarization site and surrounding tissue (Fig. 2). These intra-axonal and inward volume currents are the origin of magnetic fields. Their intensity and direction are based on Ampère's circuital law. In this article, we define the forward intra-axonal current as the leading current and the backward intra-axonal current as the trailing current.

Based on previous work (Fukuoka et al., 2002, 2004), the negative peak of the action potential in the nerve is equivalent to the inward volume current at the depolarization site. Therefore, to compare dorsal column current activity estimated from magnetic field measurement and the cervical N11 in SEPs, the timing of the inward volume current at the depolarization site flowing perpendicular to the spinal cord was compared with the SEP N11 negative peak in the C5S–left Erb's point derivation. The postero-anterior electrical current estimated from magnetic recordings was compared with the peak latency of the cervical N13 potential in the C5S–AC derivation. Electrical activity in the intervertebral foramen was evaluated using the trailing current because the inward volume currents at the depolarization site spread centripetally in the intervertebral foramen and because confronting currents produce magnetic fields that cancel each other out; the leading current can pass, even at the clipped point, according to our previous findings (Fukuoka et al., 2004).

Linear regression analysis was performed to confirm the correlation between the estimated electrical current and the SEP.

P values less than 0.05 were considered significant. All statistical analyses were performed using GraphPad Prism 5.0 for Windows (GraphPad Software, San Diego, CA).

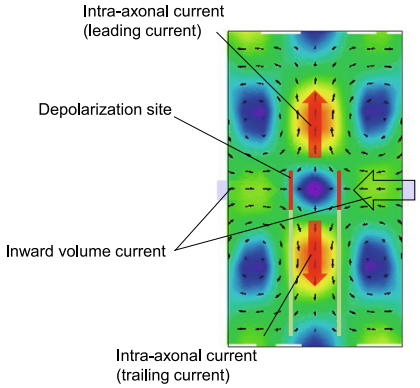

Fig. 2. Schema of the electrical currents during nerve conduction.

3. Results

3.1. Experiment 1. Recording of the magnetic field from the surface of the posterior neck in response to electrical supramaximal median nerve stimulation at the wrist

SCEFs were successfully recorded in all 16 healthy participants. The SCEFs indicated two to four phasic waveforms and Fig. 3 shows the three-directional magnetic fields recorded by each sensor in a representative participant (HC1, a 34-year-old man). The reconstructed current distribution is displayed as a pseudocolor map superimposed on an X-ray image of the participant's cervical spine. Fig. 4 shows a representative case (HC1); at a latency of 9.7 ms, leading axonal currents flowed into the C5 to C7 intervertebral foramen. At 10.3 ms, the leading axonal currents flowed into the spinal canal. Then, at 12.7 ms, trailing axonal currents, which were caudally directed, appeared in the intervertebral foramen. Following the leading axonal currents, currents flowing perpendicular to the spinal cord, indicating an inward volume current at the depolarization site in the dorsal column fibers, appeared at around the C7 level and propagated toward the cranium from 11.5 ms to 12.1 ms after the stimulus. The current waveforms were retrieved from the virtual electrodes at each vertebral level at the midline of the cervical spinal canal and the 2-cm lateral line. In Fig. 5 (HC1), the upper black traces represent SEP waveforms recorded with a C3′–Fz montage, C3′–left Erb's point montage, Fz–left Erb's point montage, and C5S–left Erb's point montage. A waveform recorded with a C5 posterior–left Erb's point montage showed a small N11 potential during the transition from the P9 potential of the brachial plexus origin to the cervical N13 potential of the dorsal horn origin. The lower waveforms represent the currents flowing perpendicular to the spinal cord, with the inward volume current at the depolarization site in the dorsal column at each positioned marked by virtual electrode. The shifts in the peak latencies of the waveforms indicated that the estimated reconstructed inward volume currents at the depolarization site in the dorsal column ascended sequentially along the spinal canal. The peak latency of the reconstructed electrical current C5 (solid red arrowhead) was almost the same as that of the N11 potential of the SEPs. Moreover, the peak latency of the reconstructed electrical current at C5 and the peak latency of the N11 SEP component recorded with a C5S–left Erb's point montage were well-correlated in all 16 participants ($r = 0.94$, $p < 0.0001$) (Fig. 6). Whereas the conduction velocity of the ascending volley could not be obtained from conventional SEP analyses, the conduction velocity of the ascending volley calculated from the peak latency of the reconstructed electrical current at the C5–6 virtual electrode could be evaluated and ranged from 53.9 to 75.9 m/s ($n = 10$; average, 63.1 ± 7.5 m/s).

In 10 of the 16 participants, the electrical activities in the intervertebral foramens (C4/5 to T1/2) were also evaluated with a trailing current because the inward volume currents at the depolarization site spread centripetally in the intervertebral foramen and because confronting currents produce magnetic fields that cancel each other out; the leading current can even pass at the clipped point, according to our previous findings (Fukuoka et al., 2004). Reconstructed currents at the adjacent intervertebral foramen (C4/5 to T1/2) are shown in Fig. 7A (from a representative case: HC2, a 39-year-old woman). The trailing axonal currents in the intervertebral foramens were estimated in all 10 of the participants. Each individual variation in the peak trailing axonal current density flowing into the intervertebral foramens is shown in Fig. 7B (HC2–11). The currents were largest at the C6/7 intervertebral foramen (outlet of root C7) or the C7/T1 intervertebral foramen (outlet of root C8) in most participants.

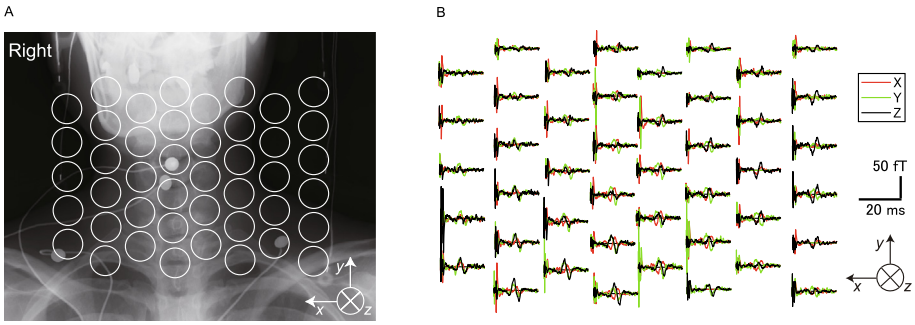

Fig. 3. Magnetic fields measured from the surface of the posterior neck in response to electrical supramaximal median nerve stimulation at the wrist. (A) Positions of the sensors superimposed on an X-ray image of a participant. (B) The three-directional magnetic fields recorded by each sensor (a representative case: HC1, a 34-year-old man). The black traces are magnetic fields in the ventral–dorsal direction relative to the cervical spinal cord (ventral is upward in the graphs). The red traces are magnetic fields in the left–right direction (right is upward). The green traces are magnetic fields parallel to the spinal cord (cranial is upward). Some malfunctioning pickup coils show a flat line. The red signals, mainly generated from intra-axonal currents, are highest above the spinal cord. The polarity of the black and green signals is reversed on each side of the spinal cord. (For interpretation of the references to colour in this figure legend, the reader is referred to the web version of this article.)

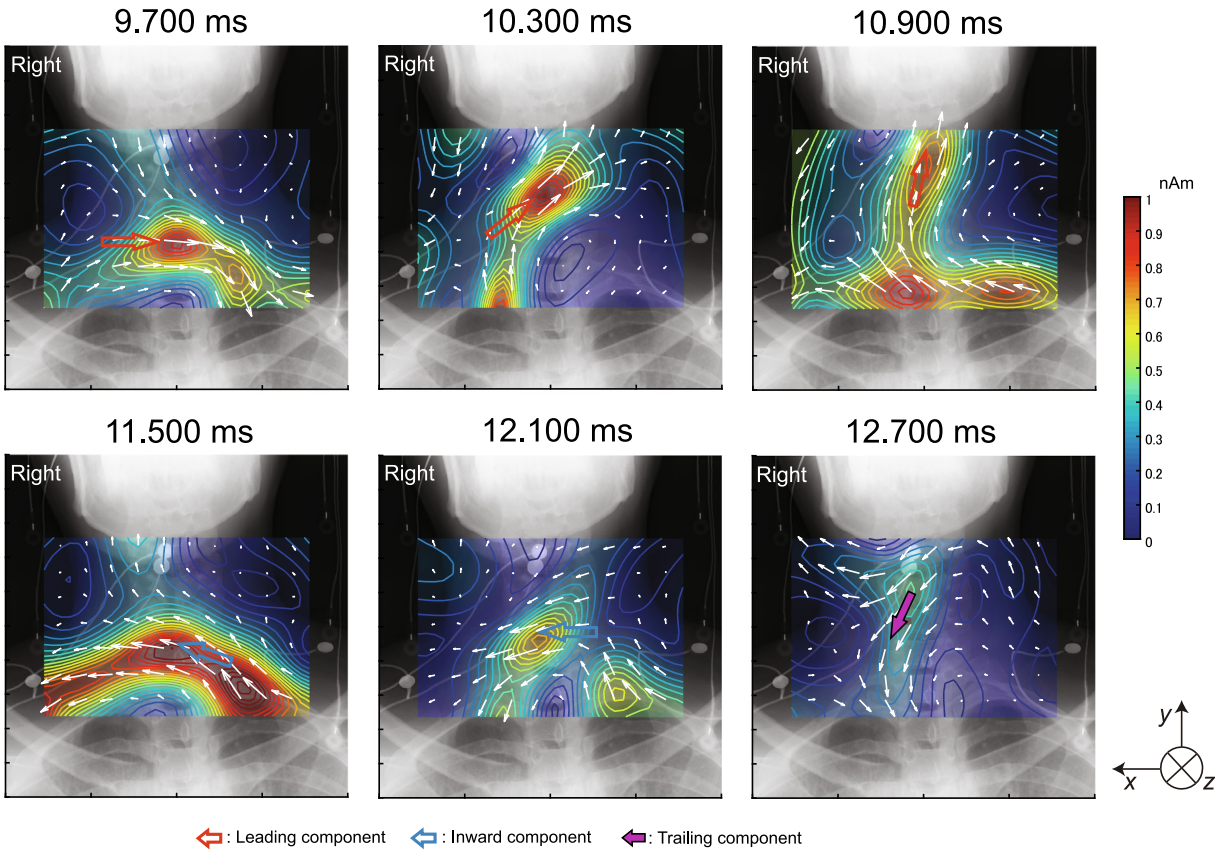

Fig. 4. Reconstructed currents estimated from the magnetic field measured from the surface of the posterior neck in response to electrical supramaximal median nerve stimulation at the wrist. Reconstructed current map (a representative case: HC1, a 34-year-old man). Currents at the level of the spinal canal are reconstructed by a recursive null-steering beamformer and superimposed on an X-ray image. The current intensity is shown by a color scale (where red is high). Small white arrows indicate current vectors. The leading component of the currents (large upward-pointing red arrow) appears 9.7 ms after stimulation and propagates cranially along the spinal canal. At 12.7 ms, the trailing component (downward-pointing red arrow) appears on the caudal side. Perpendicular currents (blue arrows) flowing toward the spine between the leading and trailing components are also observed on both sides. (For interpretation of the references to colour in this figure legend, the reader is referred to the web version of this article.)

3.2. Experiment 2. Recording of the magnetic field from the surface of the unilateral neck in response to electrical supramaximal median nerve stimulation at the wrist

SCEFs were successfully recorded in all 13 healthy participants. The magnetic fields indicated two to four phasic waveforms and Fig. 8 shows the three-directional magnetic fields recorded by each sensor in a representative participant (HC1). In Fig. 9, the reconstructed current distribution in a representative participant (HC1) 13.2 ms after stimulation is displayed as a pseudocolor map superimposed on an X-ray image of the cervical spine. The virtual electrodes, C5 posterior (C5S) electrode, and AC electrode are displayed on the lateral X-ray images of the participant. The upper traces are SEPs recorded with a C5S–AC montage that show the cervical N13–P13 potential generated by an excitatory postsynaptic potential at the dorsal horn. The lower waveforms show the

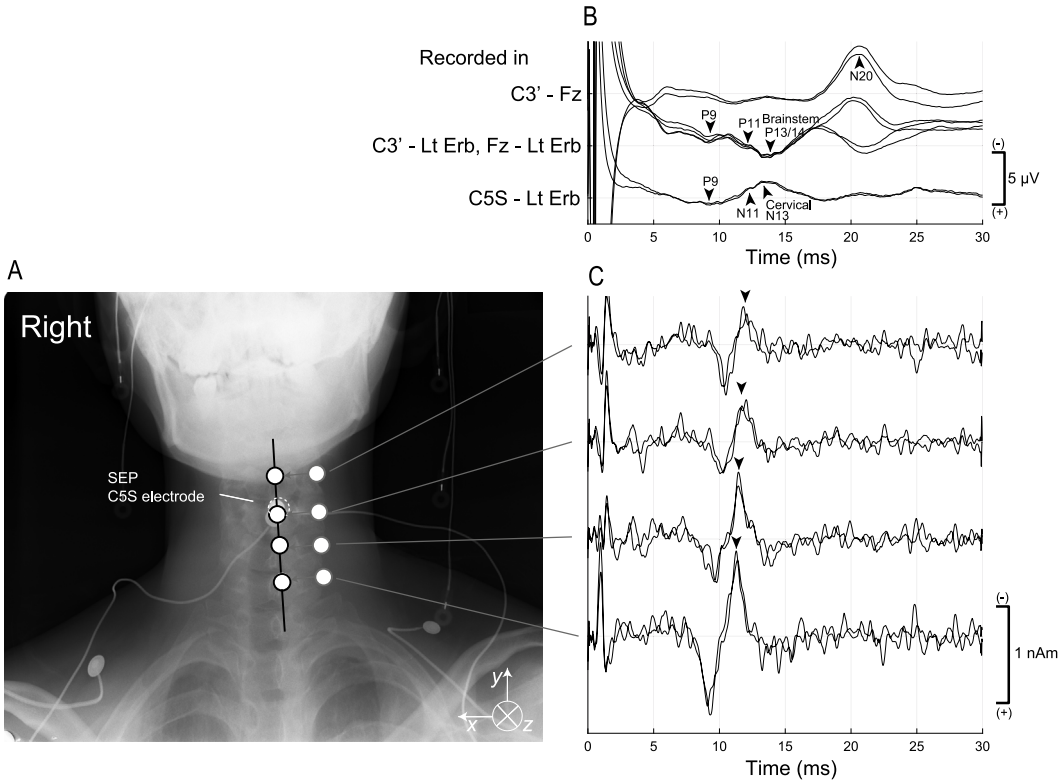

Fig. 5. Waveforms of somatosensory evoked potentials and reconstructed currents at "virtual electrodes". In a representative case (HC1, a 34-year-old man), the upper black traces represent somatosensory evoked potential (SEP) waveforms recorded with a C3′–Fz montage, C3′–left Erb's point montage, Fz–left Erb's point montage, and C5 posterior (C5S)–left Erb's point montage. The waveforms with a C5S–left Erb's point montage show a small N11 potential during the transition from the P9 potential of the brachial plexus origin to the cervical N13 potential of the dorsal horn origin. The lower waveforms represent the currents that flow perpendicular to the spinal cord, with the inward volume current at the depolarization site in the dorsal column at each position marked by a virtual electrode. The shifts in the peak latencies of the waveforms indicate that the estimated reconstructed inward volume currents at the depolarization site in the dorsal column ascend sequentially along the spinal canal. Moreover, the peak latency of the reconstructed electrical current at C5 is almost the same as that of the N11 potential of the SEPs.

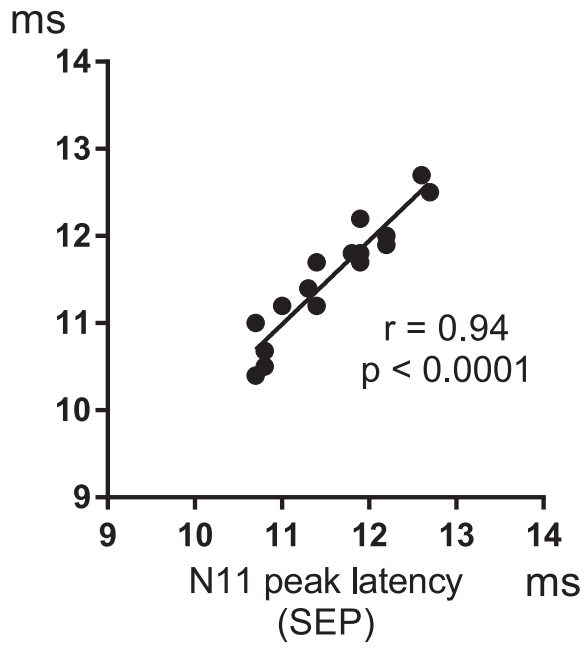

Fig. 6. Correlation between the peak latencies of the estimated electrical currents and somatosensory evoked potentials. The peak latency of the estimated electrical current perpendicular to the spinal cord at C5, which indicates the estimated inward volume current in the dorsal column at C5, and the N11 peak latency of somatosensory evoked potentials (SEPs) recorded with a C5 posterior (C5S)–contralateral Erb's point montage are well-correlated in all 16 participants ($r = 0.94$, $p < 0.0001$).

reconstituted dorsal–ventral direction currents at each virtual electrode centered around the C5 level spinal canal in the X axis (virtual electrodes X − 30, X − 15, 0, X + 15, and X + 30) and Y axis (virtual electrodes Y − 15, 0, Y + 15, and Y + 30). The estimated electrical current intensity was larger in the spinal canal at the C5 level. Moreover, the culmination of the postero-anterior electrical current estimated from the magnetic recordings coincided with the peak of the cervical N13–P13 and the volume-conducted posterior cervical negative and anterior cervical positive SEP responses in all of the 13 participants; the current peak latency was significantly correlated with the cervical N13–P13 peak latency of the SEPs ($r = 0.97$, $p < 0.0001$) (Fig. 10).

4. Discussion

In this study, we succeeded in recording SCEFs with a high signal-to-noise ratio after median nerve stimulation at the wrist. This approach permitted the visualization of complex neural activities generated from the nerve roots and the cervical spinal cord from about 9 to 13 ms after stimulation. Reconstruction of the spatial distribution of the current density around the cervical cord by UGRENS showed that median nerve SCEFs comprise three components: action currents at the dorsal root entry zone, action currents traveling along the dorsal column, and intracellular currents of the neurons within the dorsal horn.

First, we discuss the action currents at the dorsal root entry zone. The conventional electrophysiological method is inferior when evaluating the electrical activity in the intervertebral foramen. In the present study, the electrical activity in the interverte-

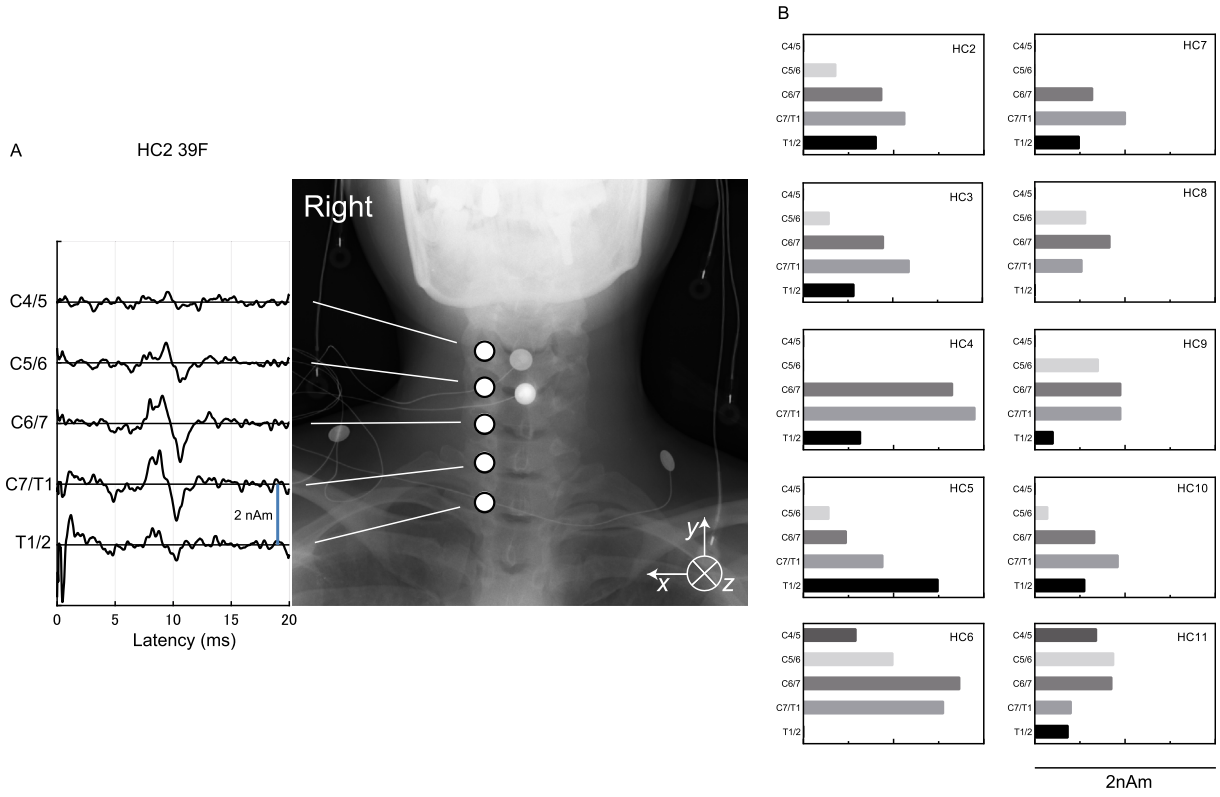

Fig. 7. Reconstructed currents estimated from the magnetic field measured at the adjacent intervertebral foramina in response to electrical supramaximal median nerve stimulation at the wrist. (A) Reconstructed currents at the adjacent intervertebral foramen (a representative case: HC2, a 39-year-old woman). (B) Each individual variation in the peak trailing axonal current density flowing into the intervertebral foramens (HC2–11). The currents are largest at the C6/7 intervertebral foramen (outlet of root C7) or the C7/T1 intervertebral foramen (outlet of root C8) in most participants. Currents passing through the C4/5 intervertebral foramen (outlet of root C5) are observed in 2 of the 10 participants, HC6 and HC11.

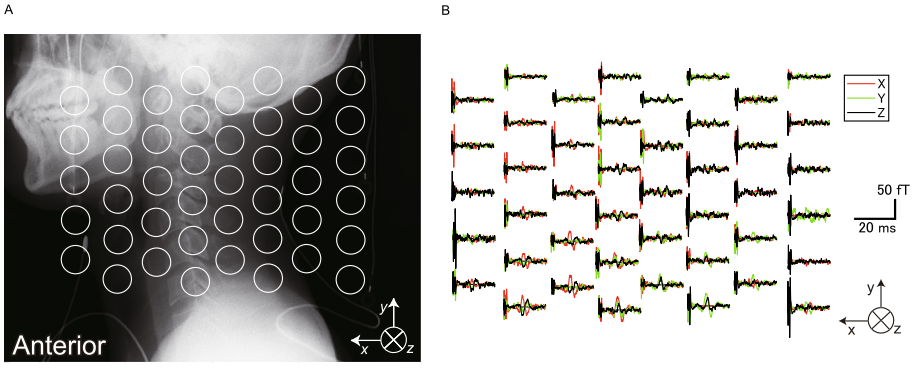

Fig. 8. Magnetic field measured from the surface of the unilateral neck in response to electrical supramaximal median nerve stimulation at the wrist. (A) Positions of the sensors superimposed on an X-ray image of a participant. (B) The three-directional magnetic fields recorded by each sensor (a representative case: HC1, a 34-year-old man). The black traces are magnetic fields in the left-right direction relative to the cervical spinal cord (left is upward in the graphs). The red traces are magnetic fields in the dorsal-ventral direction (ventral is upward). The green traces are magnetic fields parallel to the spinal cord (cranial is upward). Some malfunctioning pickup coils show a flat line. The red signals, mainly generated from intra-axonal currents, are highest above the spinal cord. The polarity of the black and green signals is reversed on each side of the spinal cord. (For interpretation of the references to colour in this figure legend, the reader is referred to the web version of this article.)

bral foramen could be evaluated by MSG. Anatomically, the median nerve is usually innervated from C6–T1 but less often from C5 (Netter, 2014). Consistent with the typical innervation pattern, the currents were largest at the C6/7 intervertebral foramen (outlet of root C7) or the C7/T1 intervertebral foramen (outlet of root C8) in most participants and currents passing through the C4/5 intervertebral foramen (outlet of root C5) were observed in 2 of the 10 participants: HC6 and HC11. Many individual differences have been reported in the dermatome in the upper limb (Kimura, 2001; Willbourn and Aminoff, 1988). Using MSG, it may be possible to easily determine individual differences in innervation. Then, by comparing the evoked magnetic fields on the affected and non-affected sides of the intervertebral foramens, it will be possible to electrophysiologically diagnose the level of the radiculopathy in the cervical spine. However, further studies are needed, including animal experiments, because the accuracy of the signal source estimation of the spatial filtering method may not be sufficient. A next-generation algorithm that has higher spatial resolution than the current one should be considered. Moreover, because median nerve electrical stimulation at the wrist activates mainly C7 and

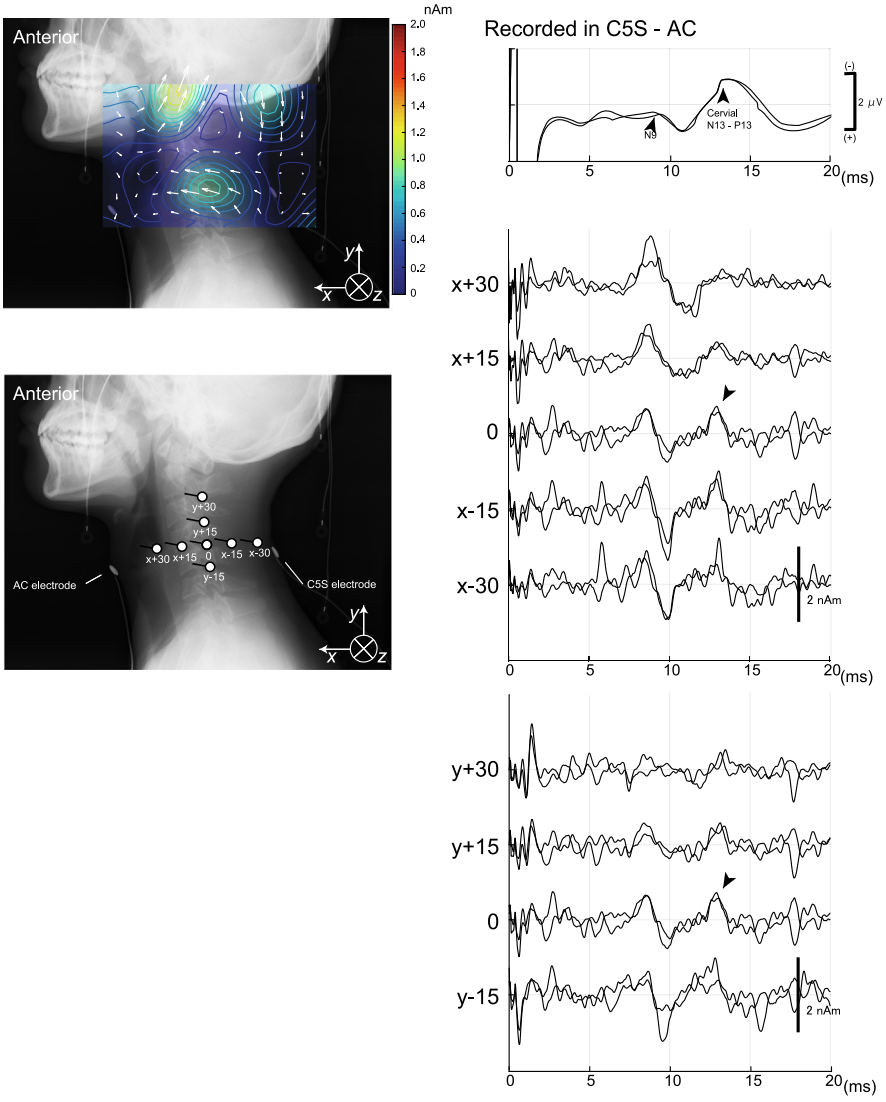

Fig. 9. Waveforms of somatosensory evoked potentials and reconstructed postero-anterior currents at a "virtual electrode". The reconstructed current distribution 13.2 ms after stimulation in a representative participant (HC1, a 34-year-old man) is displayed as a pseudocolor map superimposed on an X-ray image of the cervical spine. The virtual electrodes, C5 posterior (C5S) electrode, and anterior cervical (AC) electrode are displayed on the lateral X-ray images of the participant. The upper waves: somatosensory evoked potentials (SEPs) recorded at a C5S–AC montage. The lower waveforms: the reconstituted currents at each virtual electrode centered on the C5 level spinal canal in the X axis (virtual electrodes X − 30, X − 15, 0, X + 15, and X + 30) and Y axis (virtual electrodes Y − 15, 0, Y + 15, and Y + 30). The estimated electrical current intensity was larger in the spinal canal at the C5 level. The culmination of the estimated dorsal–ventral electrical current coincides with the peak of the cervical N13–P13 in the SEP.

C8 innervated sensory and motor nerves, our previous method can evaluate radiculopathy in C7 and C8, but is less suitable for evaluating electrical nerve activity in the C4/5 and C5/6 intervertebral foramens. Other types of nerve electrical stimulation, such as that of the superficial radial nerve and lateral antebrachial cutaneous nerve, should be considered.

The action potential propagation along the dorsal column is recorded as a small negative notch in P9 to cervical N13 waveforms with a C5S–NC derivation in the SEPs. It can also be recorded as a P11 potential with a cephalic–NC montage in about two-thirds of individuals. There is a consensus that prolonged latency or decreased amplitude of the N11 or P11 potential may indicate dorsal column dysfunction (El Negamy and Sedgwick, 1979; Restuccia et al., 1992). However, it is impossible to observe the ascending impulses and to measure the conduction velocity in SEPs. In the present study, we demonstrated using MSG that leading currents followed by trailing currents travel rostrally in the spinal canal. Between the leading axonal currents and trailing axonal currents, evaluation was also possible of currents flowing perpendicular to the long axis of the spinal canal that may originate from the inward volume current at the depolarization site of the dorsal column. Fukuoka et al. (2002, 2004) found that the negative peak of the action potential in the nerve is equivalent to the inward volume current at the depolarization site. Our group also previously reported that the peak latency of the inward volume current at the depolarization site flowing perpendicular to the brachial plexus corresponded to the peak latency of the compound nerve action potential at Erb's point (Watanabe et al., 2019). In the present study, the good correlation between the peak latency of the current flowing perpendicular to the spinal canal at C5 and that of the N11 of the SEPs indicates that the inward volume current activity at the depolarization site in the dorsal column was successfully recorded by MSG.

Moreover, the reconstructed electrical current that flowed perpendicular to the spinal cord ascended sequentially along the spinal canal and its conduction velocity in the dorsal column could

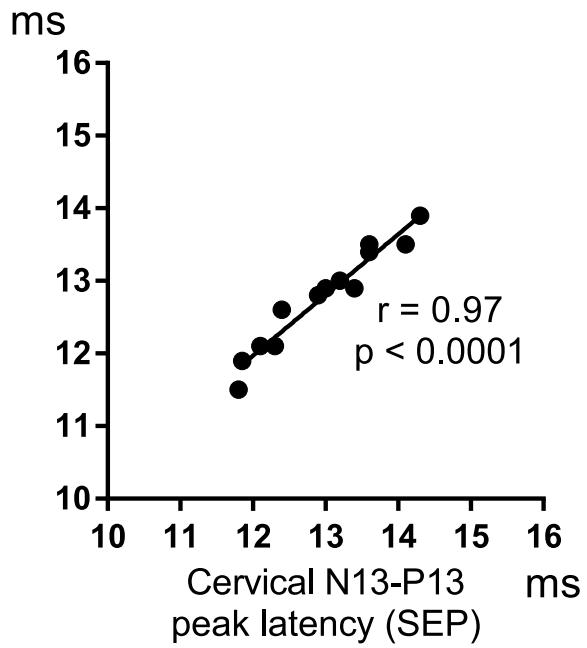

Fig. 10. Correlation between the peak latencies of the estimated electrical currents and somatosensory evoked potentials. The current density peak latency of the estimated electrical current in the posterior–anterior (dorsal–ventral) direction obtained within the spinal canal at C5 is significantly correlated with the cervical N13–P13 peak latency of the somatosensory evoked potentials (SEPs) ($r = 0.97$, $p < 0.0001$).

be evaluated. Sumiya et al. (2017) reported a conduction velocity of 64.3 m/s for reconstructed currents in response to stimulation of the lower thoracic cord. We found that the conduction velocity calculated from the peak latency at C5–6 ranged from 53.9 to 75.9 m/s (n = 10; average, 63.1 ± 7.5 m/s), which is compatible with the result of Sumiya et al. These findings indicate that magnetic field measurement with excellent spatial resolution can be applied for the detailed evaluation of the electrical activity of the dorsal column. It was reported that the evoked potential sensitivity of the detection of small lesions in multiple sclerosis was inferior to that of magnetic resonance imaging (Filippini et al., 1994). However, our results suggest that MSG might be able to identify clinically silent lesions by detecting focal slow conduction and be a more useful electrophysiological method compared with the conventional method.

One important anatomical finding is often overlooked: after spinal entry, large-diameter cutaneous afferents from mechanoreceptors such as Merkel and Meissner receptors bifurcate in the dorsal column into an ascending branch that reaches the cuneate/gracile nucleus and a shorter descending branch, as documented with horseradish peroxidase injections in the cat (Brown et al., 1980; for a review, see Abraira and Ginty, 2013). However, in the present study, as well as in all of the previous studies on MSG, descending volleys along the dorsal column could not be detected. Perhaps magnetic fields produced by the descending volleys did not persist and were cancelled out by those produced by the ascending volleys in the opposite direction that lasted longer. Instead, a not traveling but stable current source in the posterior to anterior direction could be estimated within the spinal canal at around 13 ms after the stimulus. As shown in Fig. 9, the reconstructed current source around C5 ran in the dorsal to ventral direction and its waveform was very similar to the SEPs recorded with a C5S–AC montage. This result is consistent with the results of a previous study on magnetic recording using a single-channel SQUID system by Curio et al. (1989).

Moreover, the peak intensity latency of the reconstructed current significantly correlated with the cervical N13–P13 peak latency of the SEPs in 13 healthy participants. Vertebral skin and esophageal recordings (Desmedt and Cheron, 1981; Desmedt and Nguyen, 1984; Mauguière, 1987) have revealed that the cervical N13–P13 potential is due to static transverse dipolar sources that are presumably generated from the spinal cord gray matter and dorsal horn, as evidenced by the disappearance of the cervical N13–P13 potential in patients diagnosed with syringomyelia (Urasaki et al., 1988). The equivalent current dipole of the cervical N13–P13 potential is presumably located at about the medullary C5 segments (Desmedt, 1989; Hallström et al., 1989; Jeanmonod et al., 1989). Collaterals of ascending or descending branches from large-diameter cutaneous afferents penetrate the dorsal horn through its medio-dorsal aspect and form the bushy arborizations of Cajal in cytoarchitectonic layer III (Cajal, 1995). These arborizations form dense synapses on the dendrites of interneurons, with some located in layers IV–V and with dendrites extending in parallel arrays into layer III (Brown et al., 1980; for a review, see Abraira and Ginty, 2013).

After stimulation of large-diameter cutaneous afferents in the monkey, intraspinal mapping of the lumbar spinal cord with microelectrodes located a focal excitatory postsynaptic potential negativity in the dorsal horn and positivity in the ventral cord (Beall et al., 1977). We demonstrate that, in addition to the ascending action volley along the dorsal column corresponding to the N11 or P11 potential of SEPs, MSG can evaluate stable neural activities within the dorsal horn corresponding to the cervical N13–P13 potential of SEPs. It is difficult to detect the spread of longitudinal neural activity in the spinal cord by SEP. Due to the influence of the bone and its high electrical impedance, the cervical N13 is widely distributed between C3 and T1, similar to how the cerebral N20 is widely distributed in the contralateral parietal region on the scalp. However, MSG can detect longitudinal neural activity in the spinal cord while recording the intracellular electrical current. MSG makes it possible to noninvasively measure dorsal horn activity in humans, which was previously only reported in an animal experiment (Abraira and Ginty, 2013).

5. Conclusions

We successfully and separately visualized the activities of the dorsal column, dorsal horn, and root in response to electrical median nerve stimulation at the wrist by measuring the magnetic field at the neck and reconstructing their respective currents. In contrast to the conventional electrophysiological method, MSG, due to its excellent spatial and temporal resolution after median nerve stimulation, enables us to identify the level of spinal root entry, calculate the conduction velocity of the dorsal column, and analyze segmental dorsal horn activity in detail. This approach thereby provides useful information for the functional electrophysiological diagnosis of somatosensory pathways.

Funding

This research was supported by the RICOH Company Grand Number 12500000125012A210. The funding body played no role in study design, data collection and analysis, preparation of the manuscript, or the decision to publish.

Author Contributions

M.A., S.K., I.O., and T.Y. took part in the conception and design of the project; M.A., S.K., I.O., and Y.M. were involved in its execution; and M.A., I.O., S.K, Y.M., T.W., Y. A., K.S., and Y.S. performed analysis

and interpretation of data. All authors have approved the submission of this manuscript.

Declaration of Competing Interest

None of the authors have potential conflicts of interest to be disclosed.

References

Adachi Y, Kawabata S, Fujihira J, Uehara G. Multi-channel SQUID magnetospinogram system with closed-cycle helium recondensing. IEEE Trans Appl Supercond 2017;27:1600604.

Abraira VE, Ginty DD. The sensory neurons of touch. Neuron 2013;79:618–39.

Beall JE, Applebaum AE, Foreman RD, Willis WD. Spinal cord potentials evoked by cutaneous afferents in the monkey. J Neurophysiol 1977;40:199–211.

Brown AG, Fyffe RE, Noble R. Projections from Pacinian corpuscles and rapidly adapting mechanoreceptors of glabrous skin to the cat's spinal cord. J Physiol 1980;307:385–400.

Cajal SR. Histology of the nervous system of man and vertebrates. Volume I. General principles, spinal cord, spinal ganglia, medulla and pons. Translated by Swanson N, Swanson LR. Oxford: Oxford University Press; 1995.

Cracco RQ, Cracco JB. Somatosensory evoked potential in man: far field potentials. Electroencephalogr Clin Neurophysiol 1976;41:460–6.

Cruccu G, Aminoff MJ, Curio G, Guerit JM, Kakigi R, Mauguiere F, et al. Recommendations for the clinical use of somatosensory-evoked potentials. Clin Neurophysiol 2008;119:1705–19.

Curio G, Erné SN, Sandforth J, Scheer J, Stehr R, Trahms L. Short-latency somatosensory evoked magnetic fields recorded over the brachial plexus and cervical spine in man. In: Williamson SJ, Hoke M, Stroink G, Kotani M, editors. Advances in biomagnetism. Boston: Springer; 1989. p. 133–6.

Desmedt JE. Topographic mapping of generators of somatosenseory evoked potentials. In: Maurer K, editor. Topographic brain mapping of generators of EEG and evoked potentials. Berlin: Springer Verlag; 1989. p. 76–89.

Desmedt JE, Cheron G. Central somatosensory conduction in man: neural generators and interpeak latencies of the far-field components recorded from neck and right or left scalp and earlobes. Electroencephalogr Clin Neurophysiol 1980;50:382–403.

Desmedt JE, Cheron G. Prevertebral (oesophageal) recording of subcortical somatosensory evoked potentials in man: the spinal P13 component and the dual nature of the spinal generators. Electroencephalogr Clin Neurophysiol 1981;52:257–75.

Desmedt JE, Nguyen TH. Bit-mapped colour imaging of the potential fields of propagated and segmental subcortical components of somatosensory evoked potentials in man. Electroencephalogr Clin Neurophysiol 1984;58:481–97.

El Negamy E, Sedgwick EM. Delayed cervical somatosensory potentials in cervical spondylosis. J Neurol Neurosurg Psychiatry 1979;42:238–41.

Filippini G, Comi GC, Cosi V, Bevilacqua L, Ferrarini M, Martinelli V, et al. Sensitivities and predictive values of paraclinical tests for diagnosing multiple sclerosis. J Neurol 1994;241:132–7.

Fukuoka Y, Komori H, Kawabata S, Ohkubo H, Shinomiya K. Visualization of incomplete conduction block by neuromagnetic recording. Clin Neurophysiol 2004;115:2113–22.

Fukuoka Y, Komori H, Kawabata S, Ohkubo H, Shinomiya K, Terasaki O. Imaging of neural conduction block by neuromagnetic recording. Clin Neurophysiol 2002;113:1985–92.

Hallström YT, Lindblom U, Meyerson BA, Prevec TS. Epidurally recorded cervical spinal activity evoked by electrical and mechanical stimulation in pain patients. Electroencephalogr Clin Neurophysiol 1989;74:175–85.

Hashimoto I, Odaka K, Gatayama T, Yokoyama S. Multichannel measurements of magnetic compound action fields of the median nerve in man. Electroencephalogr Clin Neurophysiol 1991;81:332–6.

Jeanmonod D, Sindou M, Mauguière F. Three transverse dipolar generators in the human cervical and lumbo-sacral dorsal horn: evidence from direct intraoperative recordings on the spinal cord surface. Electroencephalogr Clin Neurophysiol 1989;74:236–40.

Kawabata S, Komori H, Mochida K, Harunobu O, Shinomiya K. Visualization of conductive spinal cord activity using a biomagnetometer. Spine 2002;27:475–9.

Kimura J. Electrodiagnosis in diseases of nerve and muscle: Principles and practice. 3rd ed. New York: Oxford University Press; 2001. p. 628–49.

Kumihashi I, Sekihara K. Array-gain constraint minimum-norm spatial filter with recursively updated gram matrix for biomagnetic source imaging. IEEE Trans Biomed Eng 2010;57:1358–65.

Mauguière F. Short-latency somatosensory evoked potentials to upper limb stimulation in lesions of brain-stem, thalamus and cortex. Electroencephalogr Clin Neurophysiol Suppl 1987;39:302–9.

Netter FH. Atlas of human anatomy. 6th ed. Iland Ebook; 2014.

Ozaki I, Takada H, Baba M, Matsunaga M. Correlation of somatosensory central conduction time with height. Neurology 1994;44:1115–9.

Restuccia D, Di Lazzaro V, Lo Monaco M, Evoli A, Valeriani M, Tonali P. Somatosensory evoked potentials in the diagnosis of cervical spondylotic myelopathy. Electromyogr Clin Neurophysiol 1992;32:389–95.

Sasaki T, Hoshino Y, Kawabata S, Sekihara K, Adachi Y, Akaza M, et al. Visualization of electrophysiological activity at the carpal tunnel area using magnetoneurography. Clin Neurophysiol 2020;131:951–7.

Sekihara K, Nagarajan SS. Electromagnetic brain imaging: a Bayesian perspective. Cham, Switzerland: Springer International Publishing; 2015.

Sekihara K, Kawabata Y, Ushio S, Sumiya S, Kawabata S, Adachi Y, et al. Dual signal subspace projection (DSSP): a novel algorithm for removing large interference in biomagnetic measurements. J Neural Eng 2016;13:036007. https://doi.org/10.1088/1741-2560/13/3/036007.

Sumiya S, Kawabata S, Hoshino Y, Adachi Y, Sekihara K, Tomizawa S, et al. Magnetospinography visualizes electrophysiological activity in the cervical spinal cord. Sci Rep 2017;7:1064–112.

Tanosaki M, Ozaki I, Shimamura H, Baba M, Matsunaga M. Effects of aging on central conduction in somatosensory evoked potentials: evaluation of onset versus peak methods. Clin Neurophysiol 1999;110:2094–103.

Tomizawa S, Kawabata S, Komori H, Hoshino Fukuoka Y, Shinomiya K. Evaluation of segmental spinal cord evoked magnetic fields after sciatic nerve stimulation. Clin Neurophysiol 2008;119:1111–8.

Tomori M, Kawabata S, Tomizawa S, Ishii S, Enomoto M, Adachi Y, et al. Diagnosis of incomplete conduction block of spinal cord from skin surface using spinal cord evoked magnetic fields. J Orthop Sci 2010;15:371–80.

Trahms L, Erné SN, Trontelj Z, Curio G. Biomagnetic functional localization of a peripheral nerve in man. Biophys J 1989;55:1145–53.

Urasaki E, Wada S, Kadoya C, Matsuzaki H, Yokota A, Matsuoka S. Absence of spinal N13–P13 and normal scalp far-field P14 in a patient with syringomyelia. Electroencephalogr Clin Neurophysiol 1988;71:400–4.

Ushio S, Kawabata S, Hoshino Y, Adachi Y, Sekihara K, Sumiya S, et al. Visualization of the electrical activity of the cauda equina using a magnetospinography system in healthy subjects. Clin Neurophysiol 2019;130:1–11.

Watanabe T, Kawabata S, Hoshino Y, Ushio S, Sasaki T, Miyano Y, et al. Novel functional imaging technique for the brachial plexus based on magnetoneurography. Clin Neurophysiol 2019;130:2114–23.

Willbourn AJ, Aminoff MJ. AAEM Minimonograph #32: The electrophysiologic examination in patients with radiculopathies. Muscle Nerve 1988;11:1099–114.